Supplemental Material

WDR5 represents a therapeutically exploitable target for cancer stem cells in glioblastoma

Kelly Mitchell, Samuel A. Sprowls, Sonali Arora, Sajina Shakya, Daniel J. Silver, Christopher M. Goins, Lisa Wallace, Gustavo Roversi, Rachel Schafer, Kristen Kay, Tyler E. Miller, Adam Lauko, John Bassett, Anjali Kashyap, J. D'Amato Kass, Erin E. Mulkearns-Hubert, Sadie Johnson, Joseph Alvarado, Jeremy N. Rich, Eric C. Holland, Patrick J. Paddison, Anoop P. Patel, Shaun R. Stauffer, Christopher G. Hubert, Justin D. Lathia

Supplemental Material contains:

Supp. Fig. S1 includes data in support of Figure 1 and describes the spatial expression of SOX2 in GBM organoids and validation of SORE6-GFP system in GBM CSCs.

Supp. Fig. S2 includes data in support of Figure 2 and describes the spatial functional genomics screening, hits in the SOX2-depleted niche and initial testing of WDR5 inhibitor MM-102 in GBM organoids and GBM CSC sphere culture.

Supp. Fig. S3 includes data in support of Figure 3 and describes the effect of C16 on the interaction between WDR5 and WRAD complex members and properties of the WDR5 inhibitor C16.

Supp. Figs. S4 and S5 include data in support of Figure 4 and describe H3K4me3 CUT&Tag analysis of DI318 CSCs after C16 treatment.

Supp. Fig. S6 includes data in support of Figure 5 and describes the effects of C16 on GBM CSCs with high SOX2/OCT4 activity (assessed with SORE6-GFP reporter).

Supp. Fig. S7 includes data in support of Figure 6 and describes expression of WDR5 in GBM patient tumors, GBM CSC models, normal brain regions and normal brain cell types.

Supp. Fig. S8 includes data in support of Figure 7 and describes the effects of C16 on GBM CSCs and GBM organoids.

Supp. Fig. S9 includes data in support of Figure 7 and describes toxicity studies and brain penetrance of C16 in mice.

Supp. Fig. S10 is a graphical abstract showing our proposed model of WDR5 targeting in GBM CSCs**.**

Supp. Table S1 includes data in support of Figure 4 and shows the list of CUT&Tag peaks unique to each treatment group (DI318 DMSO and DI318 C16).

Supp. Table S2 includes data in support of Figure 4 and shows the list of consensus CUT&Tag peaks in DI318 DMSO and DI318 C16 groups and differential enrichment analysis of these peaks between DMSO and C16 groups by DEseq2.

Supp. Table S3 is a table of key resources used in this study.

Supplemental Figures and Legends

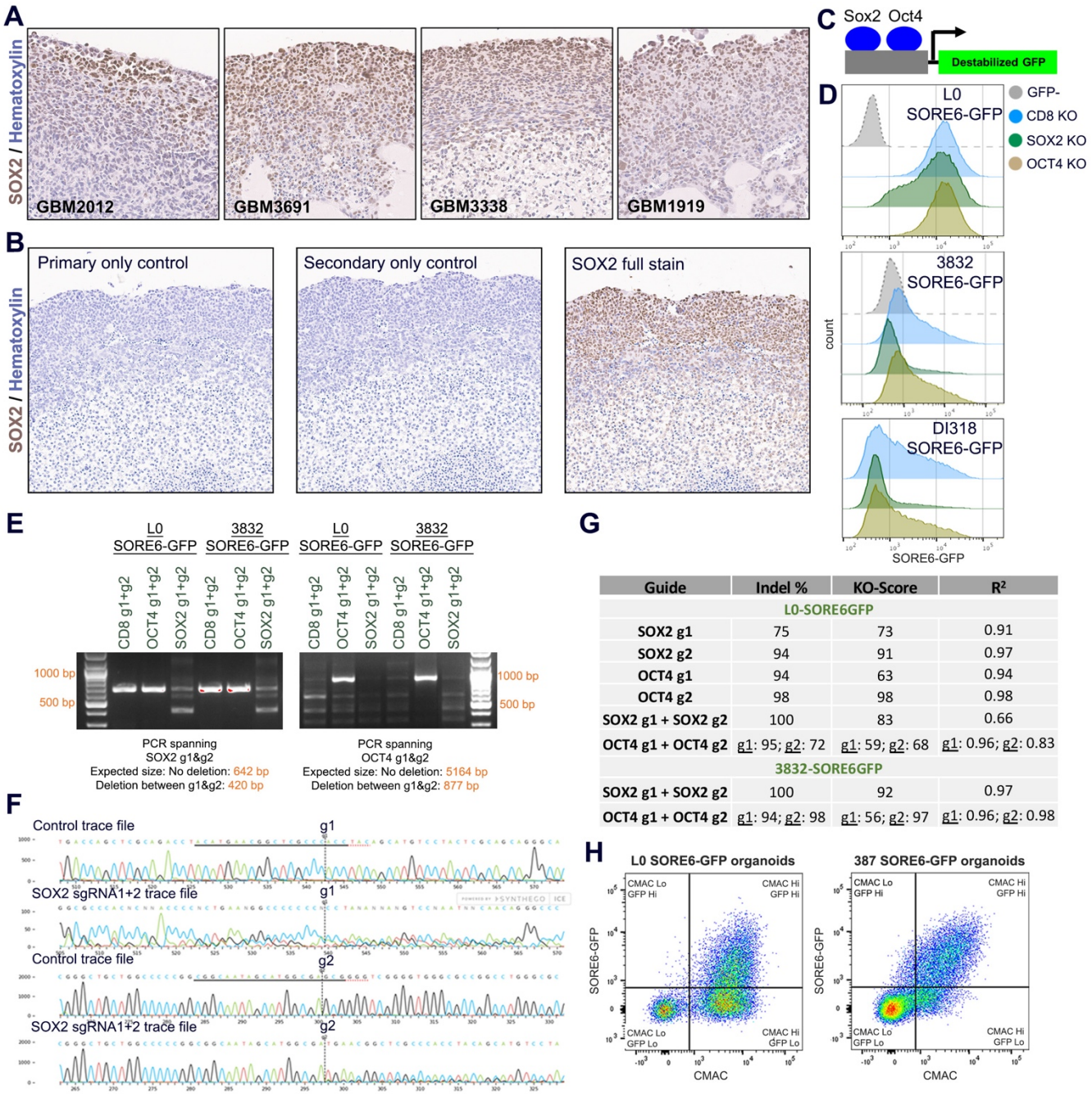

Guide	Indel %	KO-Score	R^2
	L0-SORE6GFP		
SOX2 g1	75	73	0.91
SOX2 g2	94	91	0.97
OCT4 g1	94	63	0.94
OCT4 g2	98	98	0.98
SOX2 g1 + SOX2 g2	100	83	0.66
OCT4 g1 + OCT4 g2	g1: 95; g2: 72	g1: 59; g2: 68	g1: 0.96; g2: 0.83
	3832-SORE6GFP		
SOX2 g1 + SOX2 g2	100	92	0.97
OCT4 g1 + OCT4 g2	g1: 94; g2: 98	g1: 56; g2: 97	g1: 0.96; g2: 0.98

Supplemental Figure S1 (related to Figure 1)
(**A**) SOX2 IHC of 4 different patient-derived GBM organoid specimens. 20X fields of view for individual specimens are shown. (**B**) Representative no primary antibody and no secondary antibody control stainings for SOX2 organoid IHC experiments. (**C**) Schematic describing the SORE6-GFP lentiviral reporter system. The SOX2 and OCT4 promoter response elements (cloned from the *NANOG* promoter) are fused to a destabilized GFP. (**D**) Representative flow cytometry histrograms for Fig. 1F. SOX2 and OCT4 were knocked out via CRISPR:Cas9 in SORE6-GFP transduced GBM CSCs and SORE6-GFP reporter expression was measured by flow cytometry. (**E**) PCR amplification of genomic DNA from CSCs

nucleofected with Cas9:sgRNA complexes targeting SOX2 or OCT4 7 days after nucleofection. Primers were designed in regions surrounding both CRISPR sgRNAs for SOX2 (left) and OCT4 (right) genes. A reduction in size or appearance of a PCR product indicates genomic deletion between the two sgRNA targeting sites. (**F**) Example trace files from sanger sequencing of control cells and cells nucleofected with Cas9 and a SOX2 sgRNA. Guide RNA sequence is underlined and PAM sequence is dotted underlined. (**G**) Table showing indel frequencies for cells nucleofected with Cas9 and single sgRNAs or 2 sgRNAs targeting SOX2 or OCT4 (calculated using Inference of CRISPR edits analysis (Synthego ICE tool)). Due to proximity of SOX2 guides, indel % cannot be calculated for individual guides when used simultaneously. (**H**) Representative flow cytometry plots for Fig. 1G. GBM organoids derived from SORE6GFP-transduced GBM CSCs were regionally labeled with the CellTracker Blue CMAC fluorescent dye, dissociated, and analyzed by flow cytometry to measure GFP expression in the CMAC+ outer/rim organoid niche and CMAC- inner/core niche.

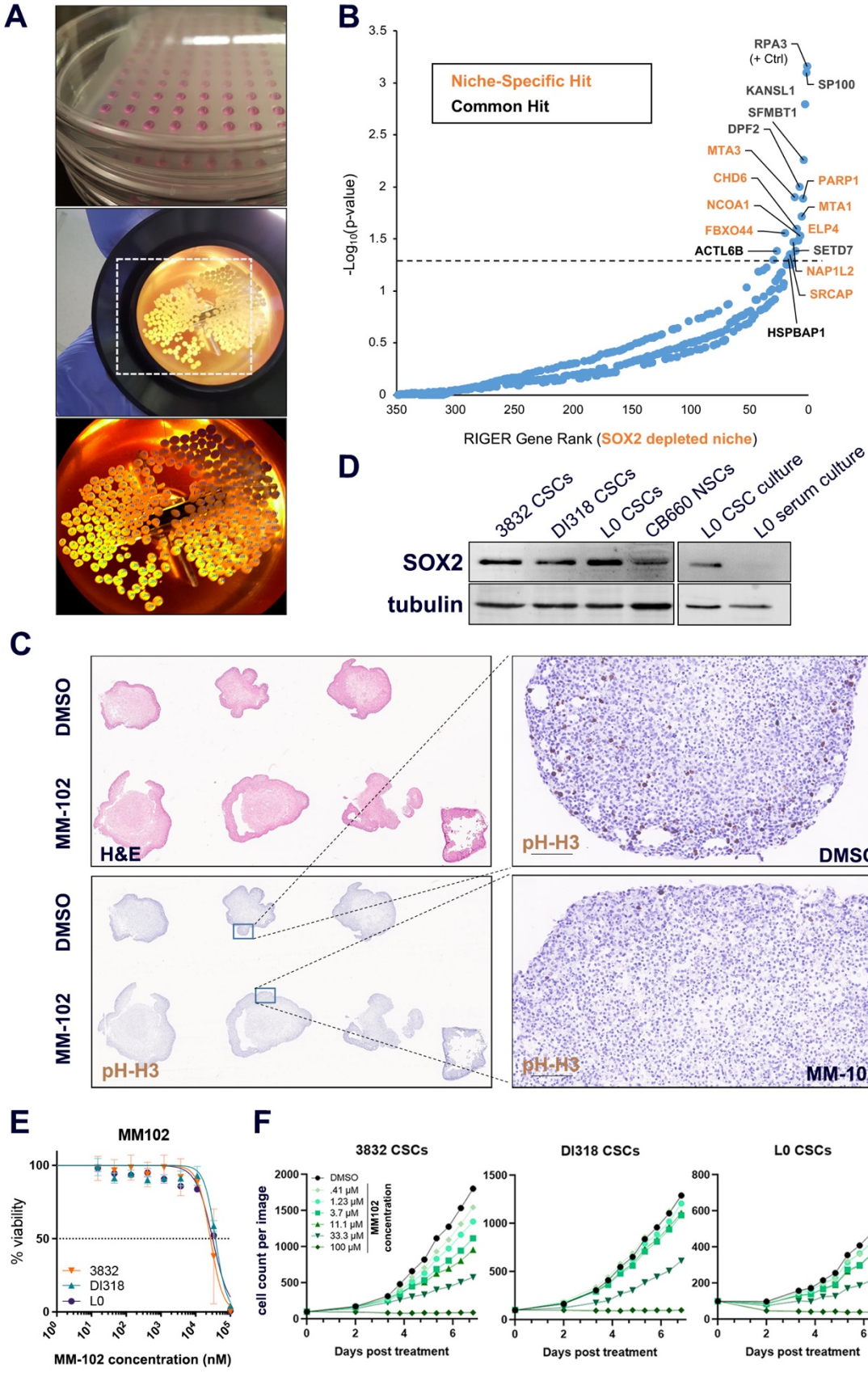
A
B
Niche-Specific Hit
Common Hit
RPA3 (+ Ctrl)
SP100
KANSL1
SFMBT1
DPF2
MTA3
CHD6
PARP1
NCOA1
MTA1
FBXO44
ELP4
ACTL6B
SETD7
NAP1L2
SRCAP
HSPBAP1
-Log10(p-value)
RIGER Gene Rank (SOX2 depleted niche)
D
3832 CSCs
DI318 CSCs
L0 CSCs
CB660 NSCs
L0 CSC culture
L0 serum culture
SOX2
tubulin
C
DMSO
MM-102
H&E
pH-H3
DMSO
DMSO
MM-102
pH-H3
pH-H3
MM-102
E
MM102
% viability
3832
DI318
L0
MM-102 concentration (nM)
F
3832 CSCs
DI318 CSCs
L0 CSCs
DMSO
.41 μM
1.23 μM
3.7 μM
11.1 μM
33.3 μM
100 μM
MM102 concentration
cell count per image
Days post treatment
Days post treatment
Days post treatment

Supplemental Figure S2 (related to Figure 2)
(**A**) Images of GBM organoid formation and example organoid cultures in a spinning bioreactor during screen outgrowth. (**B**) Rank-ordered list of genes targeted in the shRNA screen, ranked by depletion of the shRNA in the SOX2-depleted niche (CMAC-) as detected by sequencing. Dotted line represents p = 0.05 as determined by RIGER analysis of all hairpin sequences and replicates. Niche-specific hits are in orange, and common hits (including RPA3 positive control) are shown in black. (**C**) Organoids derived from GBM CSCs were treated with 63 μM MM-102 for 7 days. Low-power slide scans (left) and 20X fields of view (right) of 3 replicate organoids treated with DMSO or MM-102 showing H&E staining (top left) and phospho-histone H3 staining (right and bottom left) of GBM528 organoids. Scalebar = 100 μm. (**D**) SOX2 expression in 3 CSC models, human neural stem cells, and L0 CSCs grown in CSC-enriching culture conditions ("CSC culture") and differentiation (DMEM+10% FBS) conditions ("serum culture"). (**E**) CSCs were treated with a range of concentrations of MM-102, a peptide inhibitor of WDR5. After 7 days, viable cell counts were measured by CellTiter Glo viability assay. Values represent mean luminescence values normalized to DMSO-treated cells. (**F**) Proliferation of MM-102-treated CSCs over 7 days, determined by IncuCyte live cell imaging. Values represent mean cell count per image, n=3 technical replicates; one representative experiment is shown per CSC model.

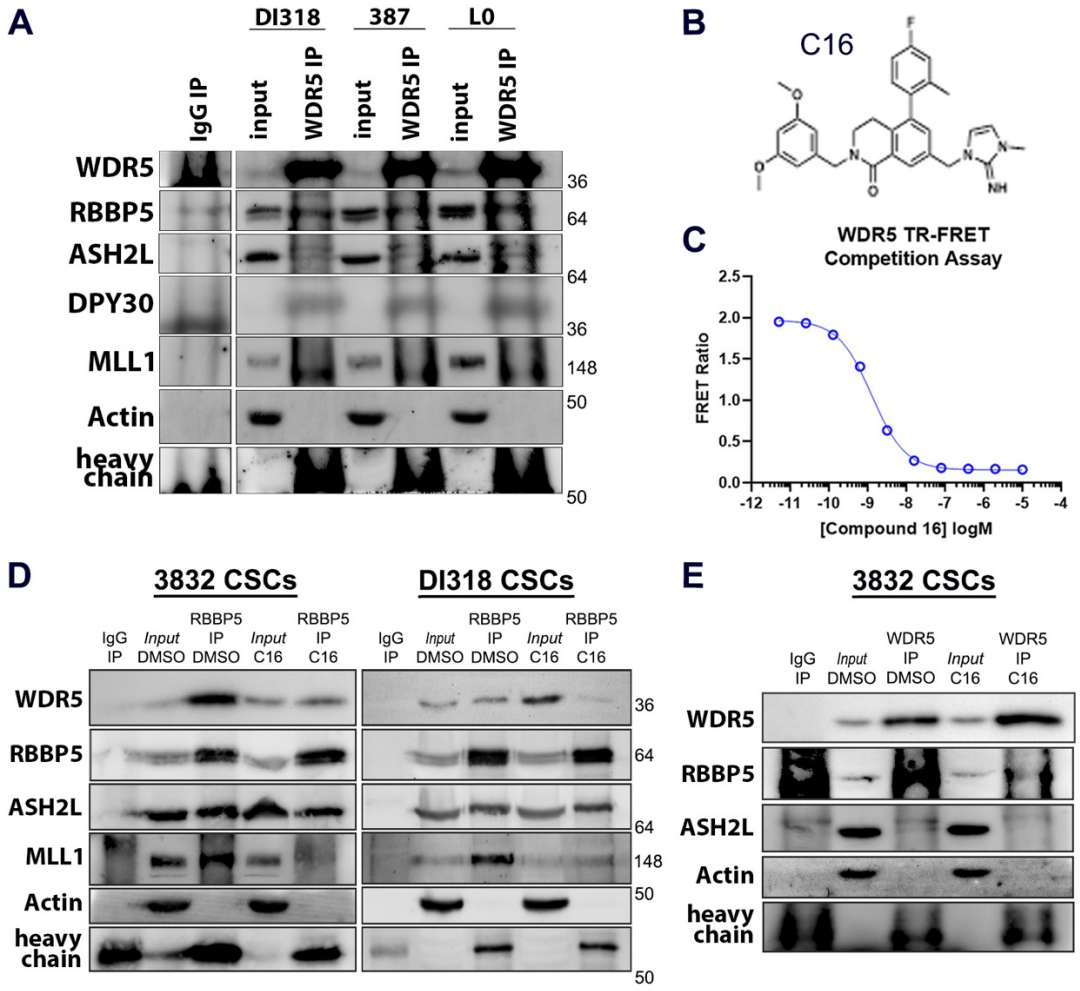

Supplemental Figure S3 (related to Figure 3)

(**A**) Immunoprecipitation of WDR5 in 3 GBM CSC models. Immunoblotting was performed for WRAD complex members and the WRAD-associated methyltransferase MLL1. Inputs are 5%. (**B**) Structure of small molecule WDR5 WIN site inhibitor C16. (**C**) Example displacement curve of C16 in WDR5 TR-FRET competition assay. Six replicates confirmed on-target binding with average Ki <20 pM as previously reported (Tian et al., 2020). (**D**) Additional blots related to Fig. 3C. Immunoprecipitation of RBBP5 after C16 inhibitor treatment (5 μM, 24 hrs) in 3832 and DI318 CSCs. Immunoblotting was performed for WRAD complex members and the WRAD-associated methyltransferase MLL1. 3832 blot - input is 5%. DI318 blot - input is 10%. (**E**) Immunoprecipitation of WDR5 after C16 inhibitor treatment (5 μM, 24 hrs) in 3832 CSCs. Immunoblotting was performed for WRAD complex members and the WRAD-associated methyltransferase MLL1. Inputs are 5%. Representative experiment is shown.

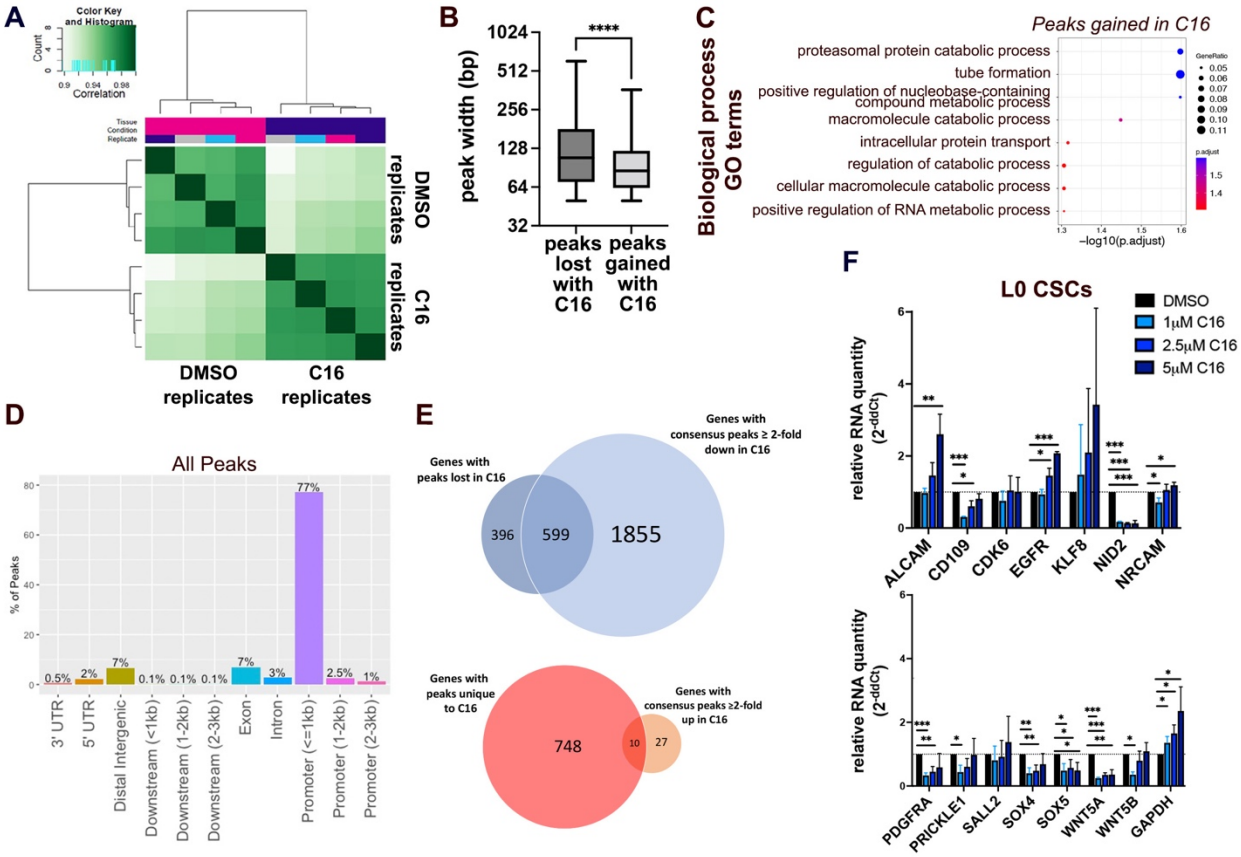

Supplemental Figure S4 (related to Figure 4)
(**A**) Hierarchically clustered correlation matrix to evaluate the relationship between CUT&Tag replicates. Pearson correlation of the log2-transformed values of read counts in each 500 bp bin between replicates. (**B**) Box and whisker plots comparing peak width for CUT&Tag peaks lost in C16 treatment group (unique to DMSO) and peaks gained in the C16 treatment group (unique to C16). P value determined by Kolmogorov–Smirnov test. (**C**) MSigDB gene set annotations enriched among CUT&Tag peaks gained in C16 treatment group (unique to C16). (**D**) Bar plot showing distribution of all consensus peaks (from DESeq2) in gene regions. (**E**) Venn diagrams showing overlap between genes with unique peaks and differential peaks in each treatment group. (**F**) qPCR for specified genes in L0 CSCs treated with indicated doses of C16 for 72 hrs. Bars represent mean expression of n=3 biological replicates, normalized to *ACTB* levels by ddCt method, +/- SD.

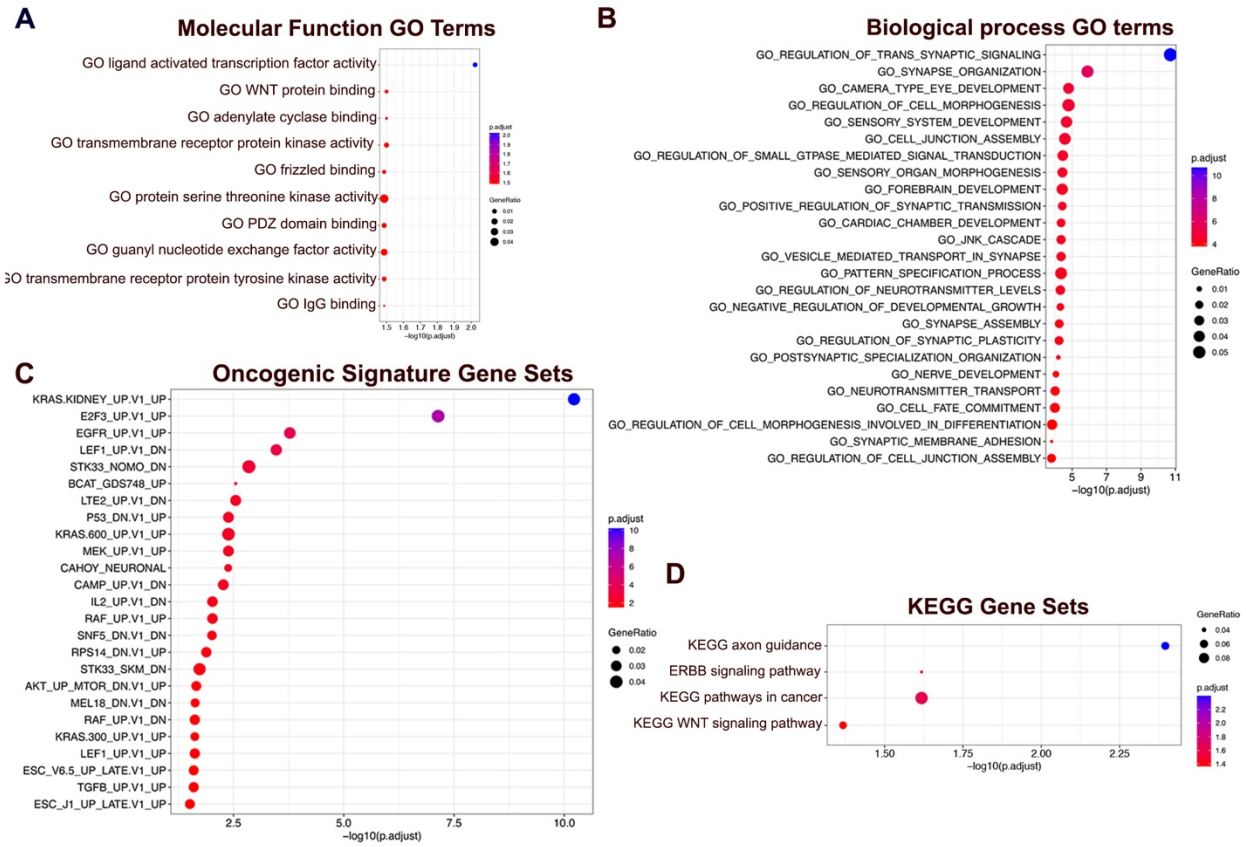

Supplemental Figure S5 (related to Figure 4)
(**A-D**) MSigDB gene set annotations enriched among CUT&Tag peaks decreased at least 2 fold (log2FC≤-1) with C16 treatment of DI318 cells.

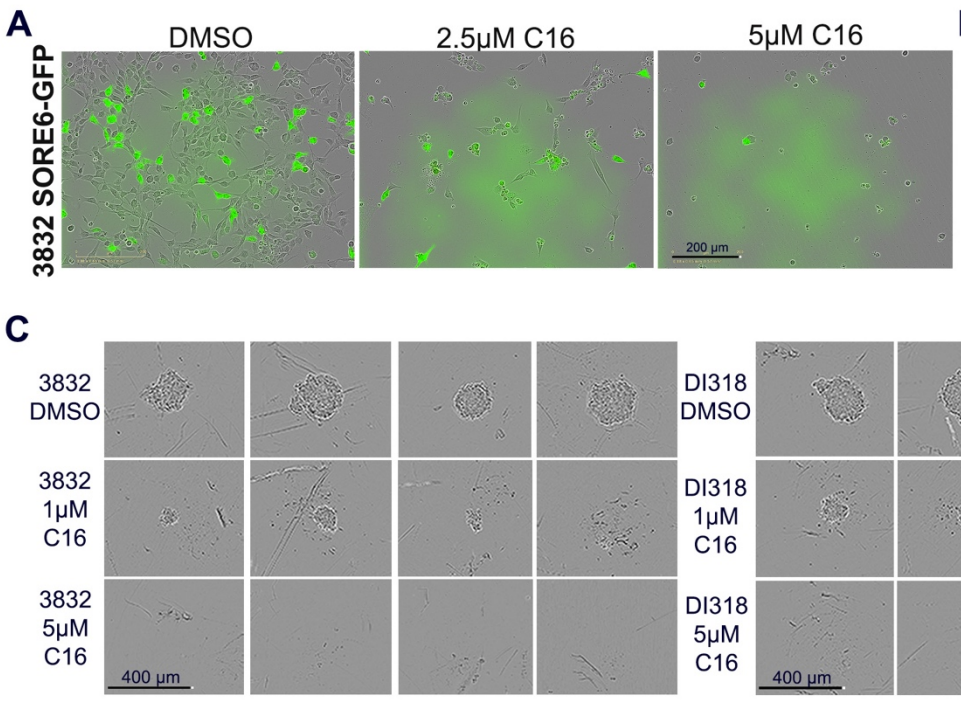

Cell model	Average sphere forming frequency	
	GFP negative	*GFP high*
DI318-SORE6GFP (n=5)	1 in 4.4	1 in 2.4
L0-SORE6GFP (n=5)	1 in 3.9	1 in 2.0

Supplemental Figure S6 (related to Figure 5)
(**A**) GBM CSC models transduced with the SORE6-GFP reporter were treated with WDR5 inhibitor C16. Representative images Day 7 post treatment are shown. (**B**) *In vitro* limiting-dilution analysis was performed on $GFP^{negative}$ and GFP^{high} populations isolated by FACS from bulk SORE6-GFP-transduced cells. Sphere-formation frequency from multiple independent replicates is shown. (**C**) *In vitro* limiting-dilution analysis was performed on CSCs in the presence of C16. Representative spheres from limiting-dilution assays at Day 10.

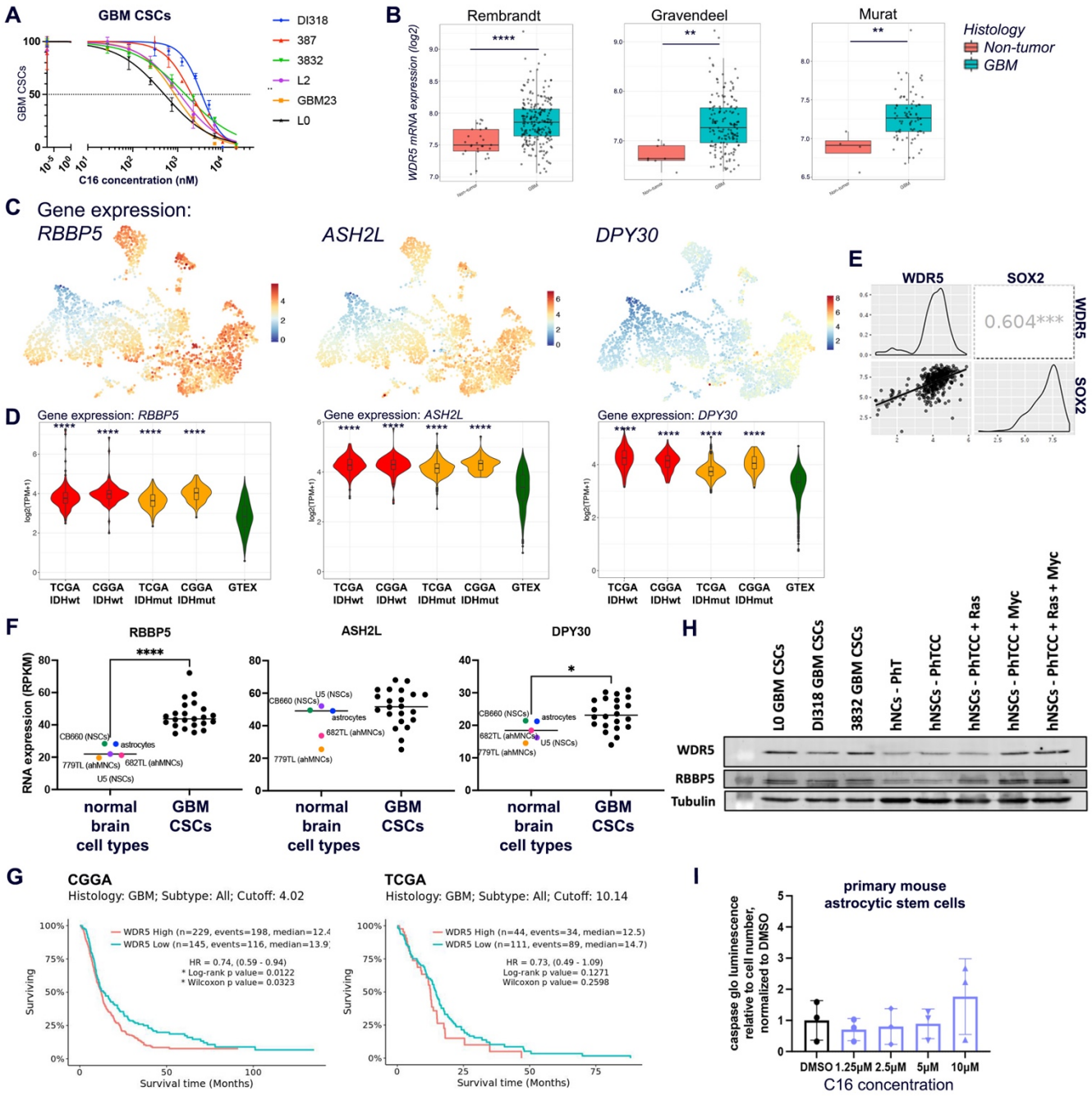

Supplemental Figure S7 (related to Figure 6)

(**A**) GBM CSCs were treated with a range of concentrations of WDR5 inhibitor C16. After 7 days, viable cell counts were measured by CellTiter Glo viability assay. Values represent mean luminescence values normalized to DMSO-treated cells. One representative curve per cell model is shown. Average IC_{50} values and number of replicates is shown in Table 1. (**B**) *WDR5* RNA expression in GBM and normal brain specimens from various RNA expression datasets. Pairwise comparisons (unpaired t-test) were performed between groups with Bonferroni corrections for multiple testing. P values; Rembrandt: p=2.0E-06; Gravendeel: p=1.4E-03; Murat: p=6.2E-03. Data obtained from the GlioVis database. (**C**) UMAP projections of gene expression for WRAD complex members on BRAIN-UMAP. Scale bar is Log2(TPM+1). (**D**) RNA expression of WRAD complex members in selected tumor and normal groups. p

values determined by unpaired t-tests with correction for multiple comparisons. (**E**) Co-expression of *WDR5* and *SOX2* in GBM from the Chinese Glioma Genome Atlas (CGGA) (n=225 wild-type IDH1 GBM samples, accessed via GlioVis database). Scatter plots (lower left), density plots (middle diagonal), Pearson's correlation coefficient with statistical significance (***p<0.001; upper right) is provided on the plot. (**F**) WRAD complex member expression from RNA sequencing of a panel of normal brain cell types and GBM lines (from (Toledo et al., 2015)). Each point represents average expression from multiple sequencing replicates. (**G**) Overall survival of GBM patients graphed based on *WDR5* expression from the CGGA and The Cancer Genome Atlas (TCGA) datasets. Accessed via GlioVis database. (**H**) WDR5 and RBBP5 expression in 3 CSC models and immortalized/transformed human neural stem cells (hNSCs). Key is in Fig. 6 legend. (**I**) Primary mouse astrocytic stem cells were treated with a range of concentrations of C16 and subjected to Caspase 3/7 Glo luminescence assay after 4 days to measure caspase 3/7 activity. Bars represent fold change in caspase 3/7 activity per cell relative to the average for DMSO-treated cells, +/- SD; circles represent biological replicates.

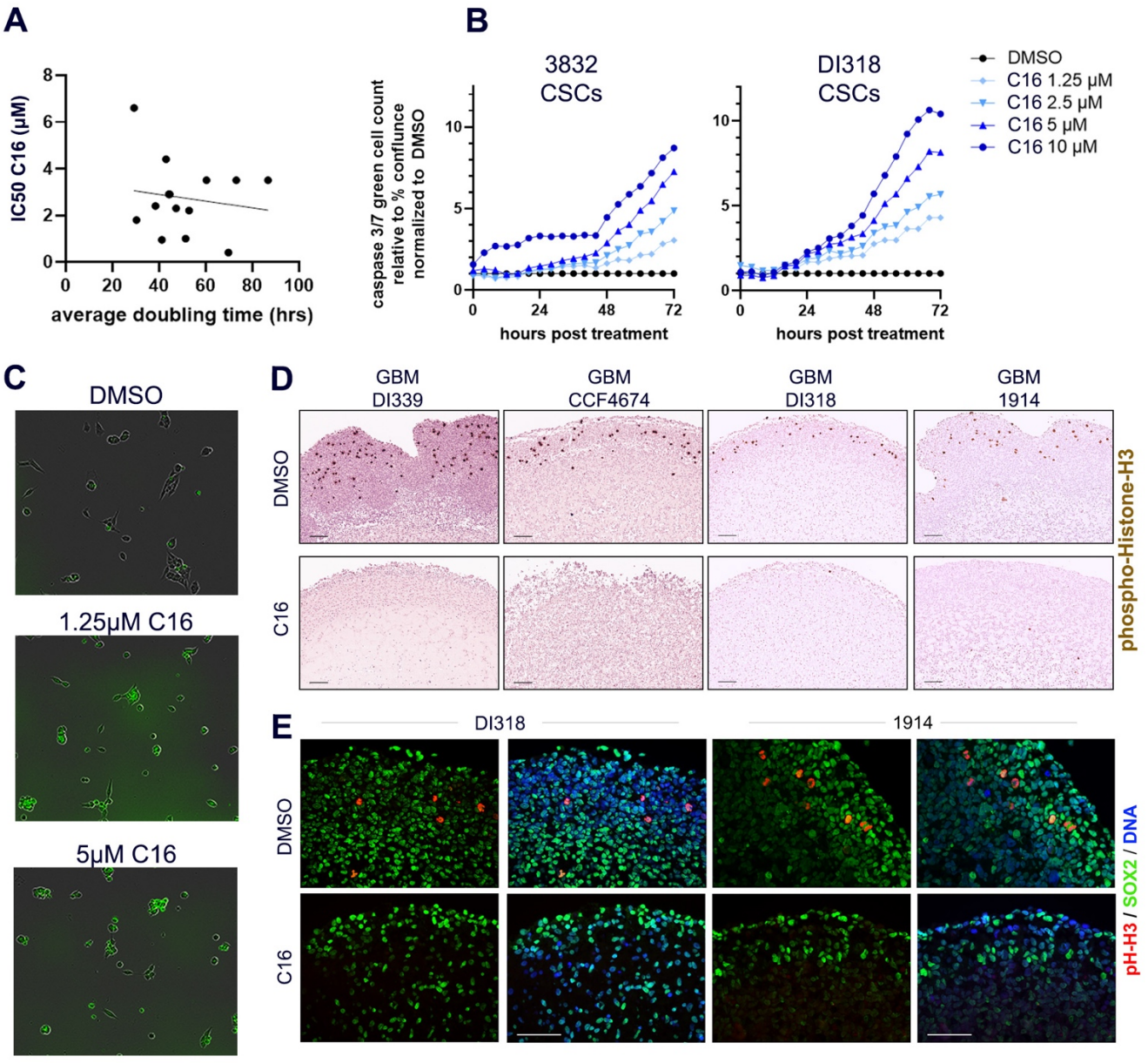

Supplemental Figure S8 (related to Figure 7)
(**A**) Doubling times and average C16 IC_{50}s are plotted for multiple CSC models and transformed neural stem cell models. Line of best fit (simple linear regression) is shown. R^2=0.022. (**B-C**) CSCs were treated with a range of concentrations of C16, and Caspase-3/7 green dye reagent (Sartorius) was added to culture medium. (**B**) Quantification of green cells (apoptotic) relative to % confluence for each dose is graphed (normalized to DMSO treatment group) over 3 days, determined by IncuCyte live cell imaging. One representative experiment is shown per CSC model. (**C**) Representative images of DI318 CSCs 4 days after treatment with C16 are shown. (**D**) IHC staining of mitotic marker phospho-histone H3 (pHH3) in 4 independent C16-treated GBM organoids (10 μM for 7 days) at 10X magnification. Scalebar = 100μm. (**E**) Immunostaining of C16-treated GBM organoids (10 μM for 7 days) for SOX2 and pHH3 to identify proliferative SOX2+ cells. Scalebar = 50μm.

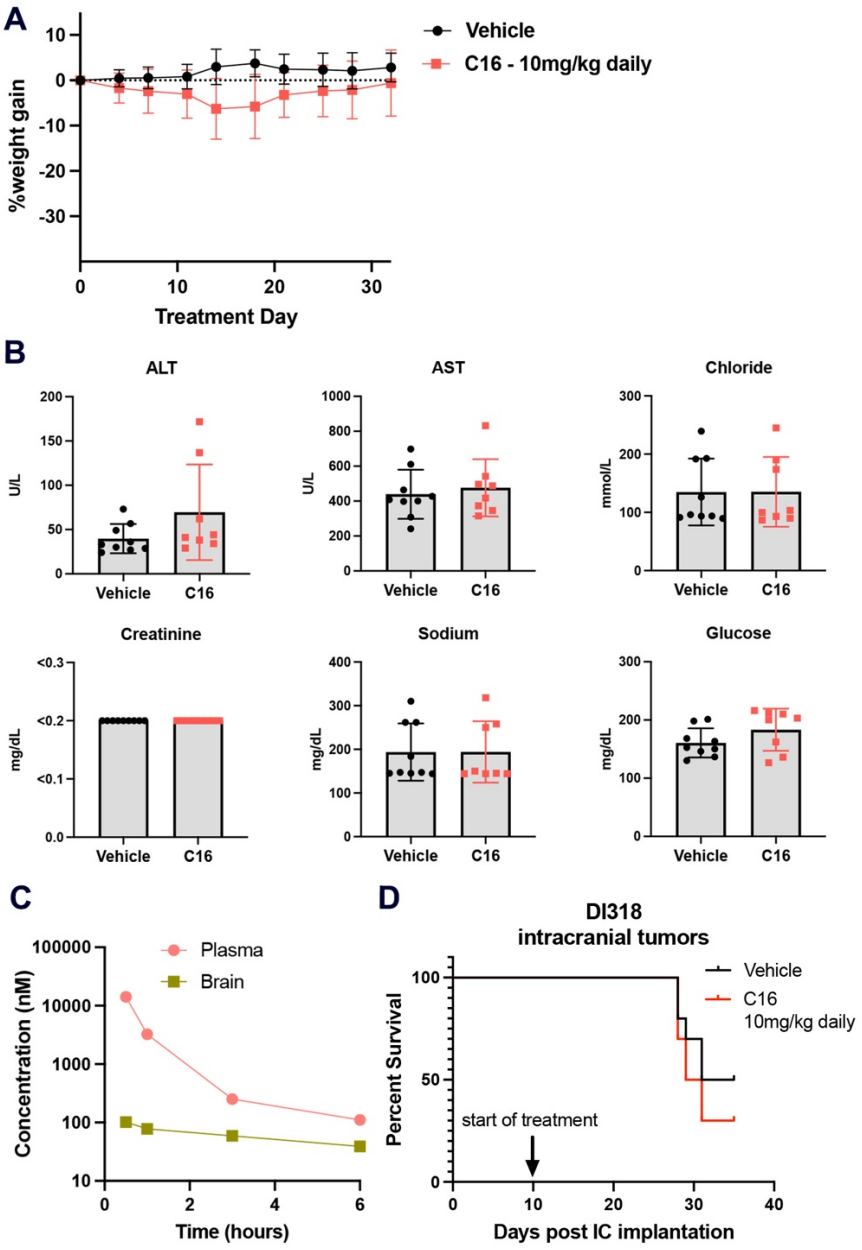

Supplemental Figure S9 (related to Figure 7)
(**A**) C16 (10 mg/kg) was injected intraperitoneally in NSG mice every day for 32 days, and mice were weighed twice weekly. (**B**) At the end of the study in (A), separated plasma was used to evaluate a basic metabolic panel using the Roche Cobas C 501 Clinical Chemistry Module. Serum concentrations of alanine aminotransferase (ALT), aspartate aminotransferase (AST), chloride, creatinine, sodium and glucose were measured, indicative of liver and kidney function. (**C**) C16 (10 mg/kg) was injected intraperitoneally in CD-1 mice, brains/plasma were collected at various time points, and the quantity of C16 in each tissue was measured by mass spectrometry. (**D**) Kaplan-Meier survival plot of mice intracranially implanted with DI318 CSCs and treated with C16 daily. n=10 per group.

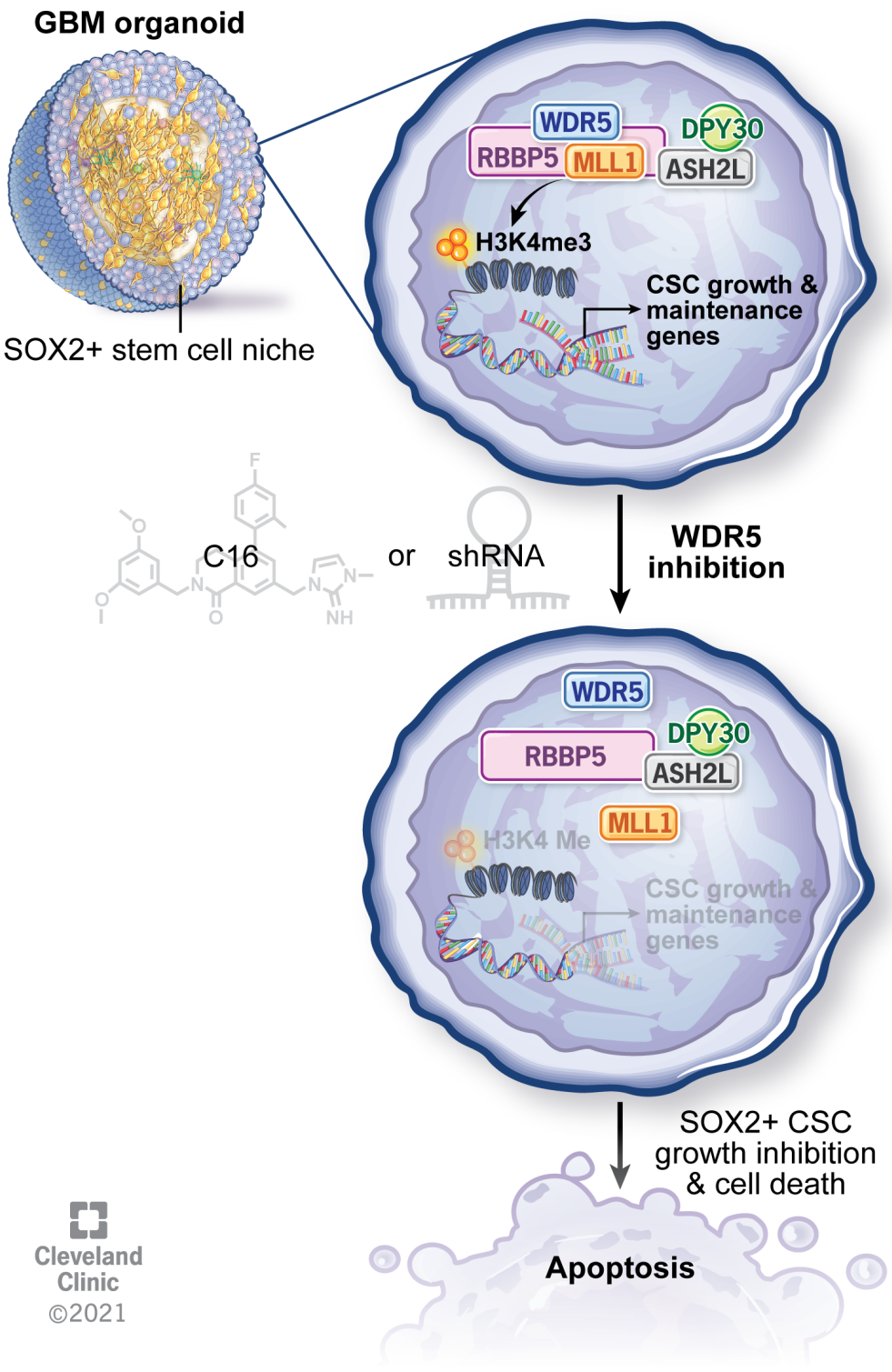

Supplemental Figure S10 (Graphical Abstract)
Proposed model of WDR5 targeting in GBM CSCs. **Top:** Described role of WDR5 and the associated WRAD complex in GBM CSCs within the SOX2+ stem cell niche. **Bottom**: Effects of WDR5 inhibition on integrity of the WRAD complex, histone methylation functions, downstream gene expression and cellular phenotypes.

Supplemental Tables and Legends

Supplemental Table S1 (excel file)
CUT&Tag peaks ≥50 bp unique to each treatment group (DI318+DMSO and DI318+C16). Data was generated with BedTools.

Supplemental Table S2 (excel file)
List of consensus CUT&Tag peaks in DI318 DMSO and DI318 C16 groups and differential enrichment analysis of these peaks between DMSO and C16 groups by DEseq2. **Sheets**: Sheet 1: shows all peaks; Sheet 2: shows only significant peaks (FDR < 0.05); Sheet 3: shows only significant peaks in C16 group (FDR < 0.05 & fold > 0); Sheet 4: shows only significant peaks in DMSO group (FDR < 0.05 & fold < 0). **Column headings**: Log2Conc: mean read concentration over all the samples (log2 normalized CUT&Tag read counts); log2(conc_C16): mean concentration over the C16 treatment group samples; log2(conc_DMSO): mean concentration over the DMSO treatment group samples; log2(ratio conc_C16/conc_DMSO): shows the difference (log2FC) in mean concentrations between the two treatment groups, with a positive value indicating enrichment in the C16 treatment group and a negative value indicating enrichment in the DMSO treatment group. Data was generated by DiffBind and DESeq2.

Supplemental Table S3 - Table of Resources

REAGENT or RESOURCE	***SOURCE***	***IDENTIFIER***
Antibodies		
mouse anti-human WDR5 (G-9)	Santa Cruz	sc-393080
rabbit anti-human RBBP5 (D3I6P)	Cell Signaling Technologies	13171
rabbit anti-human ASH2L (D93F6)	Cell Signaling Technologies	5019
mouse anti-human DPY30	Thermo Fisher	MA5-32900
hFAB Rhodamine Anti-Tubulin	Bio-Rad	12004166
hFAB Rhodamine Anti-Actin	Bio-Rad	12004167
mouse anti-human Histone H3 (96C10)	Cell Signaling Technologies	3638
rabbit anti-human Tri-Methyl-Histone H3 (Lys4) (C42D8)	Cell Signaling Technologies	9751
rabbit anti-human MLL1 (D6G8N) (Carboxy-terminal Antigen)	Cell Signaling Technologies	14197

rabbit anti-human SOX2 (D6D9) *(used for western blot)*	Cell Signaling Technologies	3579
goat anti-human SOX2 *(used for IHC/IF)*	R&D Systems	AF2018
anti-phospho-Histone-H3	Cell Signaling	9701
Biological Samples		
L0 Glioblastoma Cell Model	University of Florida (PI: Brent Reynolds)	N/A
L1 Glioblastoma Cell Model	University of Florida (PI: Brent Reynolds)	N/A
L2 Glioblastoma Cell Model	University of Florida (PI: Brent Reynolds)	N/A
DI318 Glioblastoma Cell Model (male patient)	Cleveland Clinic (PI: Chris Hubert)	N/A
DI339 Glioblastoma Cell Model	Cleveland Clinic (PI: Chris Hubert)	N/A
CCF4674 Glioblastoma Cell Model	Cleveland Clinic (PI: Chris Hubert)	N/A
GBM528 Glioblastoma Cell Model	Cleveland Clinic (PI: Jeremy Rich)	N/A
GBM1914 Glioblastoma Cell Model	Case Western Reserve University	N/A
GBM1919 Glioblastoma Cell Model	Case Western Reserve University	N/A
GBM2012 Glioblastoma Cell Model	Case Western Reserve University	N/A
T3691 Glioblastoma Cell Model	Duke University (PI: Jeremy Rich/Darrell Bigner)	N/A
T3832 Glioblastoma Cell Model (female patient)	Duke University (PI: Jeremy Rich/Darrell Bigner)	N/A
T387 Glioblastoma Cell Model	Duke University (PI: Jeremy Rich/Darrell Bigner)	N/A
T4121 Glioblastoma Cell Model	Duke University (PI: Jeremy Rich/Darrell Bigner)	N/A
GBM23/23M Glioblastoma Cell Model	MD Anderson (PI: Erik Sulman)	N/A
BT124 Glioblastoma Cell Model	University of Calgary (PI: Sam Weiss)	N/A

GBM3338 Glioblastoma Cell Model (pediatric)	Cleveland Clinic (PI: Chris Hubert)	N/A
HSJD-pGBM-001 Pediatric Glioblastoma Cell Model	Hospital Sant Joan de Deu	N/A
HSJD-DIPG-007 Diffuse Intrinsic Pontine Glioma Cell Model	Hospital Sant Joan de Deu	RRID:CVCL_VU70
CB660 Transformed human neural stem cells with addition of oncogenes (dominant-negative $p53^{DD}$ and hTERT, CyclinD1 and $CDK4^{R24C}$, c-Myc and H-RasV12)	Fred Hutchinson Cancer Research Center (PI: Chris Hubert/Patrick Paddison) (Hubert et al., 2013)	
Primary mouse astrocytic stem cells	This paper (primary cells)	
Primary human astrocytes (hTERT immortalized)	Cleveland Clinic (PI: Justin Lathia)	
U5 human neural stem cells	Fred Hutchinson Cancer Research Center (PI: Patrick Paddison)	
CB660 human neural stem cells	Fred Hutchinson Cancer Research Center (PI: Patrick Paddison)	
IMR90 human fibroblasts	ATCC	CCL-186
Chemicals, Peptides, Recombinant Proteins, Reagents & Other Materials		
CellTracker Blue CMAC	Invitrogen Molecular Probes	C2110
Doxycycline	Sigma-Aldrich	
Compound 16 (C16)	Cleveland Clinic Foundation First reported in (Tian *et al.*, 2020)	
OICR-9429	Thomas Scientific	C817G46
Piribedil dihydrochloride	TOCRIS	1031
MM-102	TOCRIS	5307
hydroxypropyl beta cyclodextran (HP-β-CD)	Sigma	C0926
Neurobasal Medium minus phenol red	Gibco	12349015
Neurobasal Medium with phenol red	Gibco	21103049

B27-supplement w/o Vitamin A	Life Technologies	12587010
Sodium Pyruvate	Life Technologies	11360070
EGF recombinant protein	R&D Systems	236-EG
FGF2 recombinant protein	R&D Systems	4114-TC
Penicillin-Streptomycin (10,000 U/mL)	ThermoFisher Scientific	15140122
Advanced DMEM-F12	Gibco	12634010
NeuroCult NS-A Basal Medium	Stem Cell Technologies	5750
N-2 Supplement	Gibco	17502048
Matrigel Basement Membrane Matrix	Corning	354234
500mL Spinner flask	Corning	3578
35mm dishes (for confocal)	MatTek	P35G-1.5-10-C
Geltrex	Life Tech	a1413202
Laminin	Sigma	L2020
Accutase cell detachment solution	Millipore Sigma/ Chemicon	SCR005
Papain Dissociation System	Worthington Biochemical	LK003150
FuGENE® HD Transfection Reagent	Promega	E2311
PEG*it* virus precipitation solution	System Biosciences	LV810A-1
SpCas9	Aldevron	9212
Protease Inhibitor Cocktail	Sigma	p8340
Phosphatase Inhibitor Cocktail	Sigma	p5726
Protein A/G agarose beads	Santa Cruz	sc-2003
Bradford Reagent (Bio-Rad Protein Assay Dye Reagent Concentrate)	Bio-Rad	5000006
PVDF membranes	EMD Millipore	ISEQ00010
RNAeasy mini kit	Qiagen	74004
Direct-zol RNA miniprep kit	Zymo Research	R2053
E.Z.N.A. MicroElute Genomic DNA Kit.	Omega Biotek	D3096-02
PhaseLock tubes	5prime	
Monarch PCR & DNA Cleanup Kit	NEB	T1030L
Phusion High-Fidelity DNA Polymerase	NEB	M0530

Power SYBR™ Green PCR Master Mix	Applied Biosystems	4367659
Critical Commercial Assays		
SG Cell Line 96-well Nucleofector™ Kit	Lonza	V4SC-3096
Caspase-Glo 3/7 assay	Promega	g8091
Incucyte Caspase-3/7 Dye for Apoptosis	Sartorius	4440
CellTiter-Glo Luminescent Cell Viability Assay	Promega	G7572
CUT&Tag-IT Assay Kit	Active Motif	53160
BBB Penetration assay	Absorption Systems	#EA203
Experimental Models: Organisms/Strains		
NSG mice (NOD.Cg-*Prkdc*^{scid} *Il2rg*^{tm1Wjl}/SzJ)	Jackson Laboratory	Stock 005557
CD-1 mice	Charles River	Strain 022
C57BL/6 mice	Jackson Laboratory	Stock 000664
Oligonucleotides		
Barcoded primers for shRNA amplification and sequencing (for screen)	(Miller et al., 2017)	p7+loop, 5′-CAAGCAGAAGACGGCATACGA-NNNN (4 nucleotide barcode)-TAGTGAAGCCACAGATGTA-3′; p5+miR3′, 5′-AATGATACGGCGACCACCGATGGATGTGGAATGTGTGCGAGG-3′
Sequencing primer for deep sequencing libraries	(Miller *et al.*, 2017)	miR30EcoRISeq, 5′-TAGCCCCTTGAATTCCGAGGCAGTAGGCA-3′
Human SOX2 CRISPR g1&g2 indel analysis primers	This paper	F: 5’- CAACCAGAAAAACAGCCCGG-3’ R: 5’- GACTTGACCACCGAACCCAT-3’
Human OCT4 CRISPR g1 indel analysis primers	This paper	F: 5’-TGATCCTCGGACCTGGCTAA-3’ R: 5’-TCACCGGCAGTTGTCTCTTC-3’
Human OCT4 CRISPR g2 indel analysis primers	This paper	F: 5’-TCCCGAATGGAAAGGGGAGA-3’ R: 5’-GTGGTGGTGTGAAAAGGCAG-3’
Human ACTIN qPCR primers	Lathia Laboratory	F: 5’-ACCTTCTACAATGAGCTGCG-3’ R: 5’-CCTGGATAGCAACGTACATGG-3’
Human ALCAM qPCR primers	(He et al., 2017)	F: 5’-ACTTGACGTACCTCAGAATCTCA-3’ R: 5’-CATCGTCGTACTGCACACTTT-3’
Human CD109 qPCR primers	Origene	F: 5’-CCTCCTAATACAGTGACTGGCAG-3’ R: 5’-CTGTTCACCACAGCCATAAGGC-3’

Human CDK6 qPCR primers	Origene	F: 5'-GGATAAAGTTCCAGAGCCTGGAG-3' R: 5'-GCGATGCACTACTCGGTGTGAA-3'
Human EGFR qPCR primers	Origene	F: 5'-AACACCCTGGTCTGGAAGTACG-3' R: 5'-TCGTTGGACAGCCTTCAAGACC-3'
Human GAPDH qPCR primers	Lathia Laboratory	F: 5'-CAATGACCCCTTCATTGACC-3' R: 5'-GACAAGCTTCCCGTTCTCAG-3'
Human KLF8 qPCR primers	Origene	F: 5'-CCTGAAAGCTCACCGCAGAATC-3' R: 5'-TGCTTGCGGAAATGGCGAGTGA-3'
Human NID2 qPCR primers	Origene	F: 5'-GCCCGGTCAAAGAGGATTCA-3' R: 5'-TGCGCACTCACAGGTGTAAT-3'
Human NRCAM qPCR primers	(Ling et al., 2019)	F: 5'-GAGCGAAGGGAAAGCTGAGA-3' R: 5'-ACAATGGTGATCTGGATGGGC-3'
Human PDGFRA qPCR primers	(Haller et al., 2007)	F: 5'-TGTCCTGGTTGTCATTTG-3' R: 5'-CTTCAACCACCTTCCCAAAC-3'
Human PRICKLE1 qPCR primers	(Jiang et al., 2021)	F: 5'-TGCTGCCTTGAGTGTGAAAC-3' R: 5'-CACAAGAAAAGCAGGCTTCC-3'
Human SALL2 qPCR primers	Origene	F: 5'-GGCTTGCCTTATGGTATGTCCG-3' R: 5'-TGGCACTGAGTGCTGTTGTGGA-3'
Human SOX4 qPCR primers	Origene	F: 5'-GACATGCACAACGCCGAGATCT-3' R: 5'-GTAGTCAGCCATGTGCTTGAGG-3'
Human SOX5 qPCR primers	(Pan et al., 2020)	F: 5'-AGGTTTGGACTCACTTGACAGG-3' R: 5'-TCCATCTGCTTCCCCATACG-3'
Human WNT5A qPCR primers	Origene	F: 5'-TACGAGAGTGCTCGCATCCTCA-3' R: 5'-TGTCTTCAGGCTACATGAGCCG-3'
Human WNT5B qPCR primers	Origene	F: 5'-CAAGGAATGCCAGCACCAGTTC-3' R: 5'-CGGCTGATGGCGTTGACCACG-3'
Recombinant RNA/DNA		
CRISPR sgRNA: CD8Ag1	(Kuppers et al., 2022) synthesized by Synthego	GUGUCGUCAGUGCACACGAG
CRISPR sgRNA: CD8Ag2	(Kuppers *et al.*, 2022) synthesized by Synthego	GCCCUUGGCCGGGACUUGTG
CRISPR sgRNA: SOX2g1	Designed with CRISPick, synthesized by Synthego	ACAUGAACGGCUCGCCCACC
CRISPR sgRNA: SOX2g2	Designed with CRISPick, synthesized by Synthego	CGGCAAUAGCAUGGCGAGCG
CRISPR sgRNA: OCT4g1	(Shin et al., 2022) synthesized by Synthego	GAAGCUCACUUGCCUCCUCC
CRISPR sgRNA: OCT4g2	Designed with CRISPick, synthesized by Synthego	CCCACCAAAUAGAACCCCCA
pPACKH1 HIV Lentivector Packaging Kit	System Biosciences	LV500A-1
SORE6-dsCopGFP lentiviral plasmid	Wakefield Lab (NIH) (Tang et al., 2015)	

pLKO.1-puro Non-Mammalian shRNA plasmid	Sigma MISSION®	SHC002
pLKO.1-puro WDR5 shRNA plasmids	Sigma MISSION®	clone IDs: TRCN0000157812 (shWDR5#12) and TRCN0000118047 (shWDR5#47)
pMD2.G packaging vector	Addgene	12259
psPAX2 packaging vector	Addgene	12260
Deposited Data		
Human reference genome NCBI build 38, GRCh38	Genome Reference Consortium	http://www.ncbi.nlm.nih.gov/projects/genome/assembly/grc/human/
Raw and analyzed data	This paper	GEO: GSE199110
Software and Algorithms		
GraphPad Prism 8 & 9	GraphPad	https://www.graphpad.com/scientific-software/prism/
Adobe Photoshop 2021	Adobe Systems	
CRISPick	Broad Institute	https://portals.broadinstitute.org/gppx/crispick/public
ICE analysis	Synthego	ice.synthego.com
ImageJ 1.53k	NIH	https://imagej.nih.gov/ij/
Incucyte S3 Software	Sartorius	
ImageScope software	Leica	
Galaxy Software	Galaxy Training Network	https://usegalaxy.org/
RNAi Gene Enrichment Ranking (RIGER) analysis	Broad Institute (Luo et al., 2008)	https://software.broadinstitute.org/GENE-E/extensions.html
DepMap portal	Broad Institute (Dempster et al., 2019; Ghandi et al., 2019; Meyers et al., 2017)	https://depmap.org/portal/
Extreme Limiting Dilution Analysis (ELDA)	(Hu and Smyth, 2009)	http://bioinf.wehi.edu.au/software/elda/index.html
GlioVis	(Bowman et al., 2017)	http://gliovis.bioinfo.cnio.es/
Bowtie2 v2.4.2	(Langmead and Salzberg, 2012)	http://bowtie-bio.sourceforge.net/bowtie2/index.shtml
FastQC v0.11.9	Simon Andrews, Babraham Bioinformatics	https://www.bioinformatics.babraham.ac.uk/projects/fastqc/
MACS2 v2.2.6	(Zhang et al., 2008)	https://pypi.org/project/MACS2/
ChIPseeker	(Yu et al., 2015)	https://bioconductor.org/packages/release/bioc/html/ChIPseeker.html
BEDTools v2.29.2	(Quinlan and Hall, 2010)	https://bedtools.readthedocs.io/en/latest/index.html#

SAMtools v1.11	(Li et al., 2009)	http://www.htslib.org/
Integrative Genomics Viewer (IGV version 2.4.8)	Integrative Genomics Viewer (IGV version 2.4.8)	IGV.org
DiffBind	(Ross-Innes et al., 2012)	https://bioconductor.org/packages/devel/bioc/vignettes/DiffBind/inst/doc/DiffBind.pdf
DESeq2	(Love et al., 2014)	https://bioconductor.org/packages/release/bioc/html/DESeq2.html
Molecular Signatures Database (MSigDB) v7.5.1	Broad Institute	https://www.gsea-msigdb.org/gsea/index.jsp
HOMER v4.11	(Heinz et al., 2010)	http://homer.ucsd.edu/homer/ngs/peakMotifs.html
R v4.1.2	R Core Team	https://www.r-project.org
R package – tidyverse	CRAN	https://cran.r-project.org/web/packages/tidyverse/index.html
R package – ggplot2	CRAN	https://cran.r-project.org/web/packages/ggplot2/index.html
R package - pacman	CRAN	https://cran.r-project.org/web/packages/pacman/index.html

Supplemental Experimental Procedures

EXPERIMENTAL MODEL AND SUBJECT DETAILS

Animals

For flank and intracranial tumor experiments, NSG mice (NOD.Cg-*Prkdc*^{scid} *Il2rg*^{tm1Wjl}/SzJ; stock 005557; Jackson Laboratory) were bred in house (Cleveland Clinic). For DI318 intracranial tumor experiments, 7.5-week-old NSG mice were used. For DI318 flank tumor experiments, NSG mice at least 8 weeks of age were used. For L0 flank tumor experiments, 8-week-old NSG mice were used. An equal number of male and female mice were used for all animal experiments and were evenly distributed between experimental groups. For the IP dosing weight study, 8-week-old C57BL/6 mice (stock 000664; Jackson Laboratory) were used. Mice were housed in the Cleveland Clinic Biological Resources Unit. Mice were maintained on a 12-hour light cycle (0600-1800). Room temperature was monitored daily and maintained at 22-25°C. All experiments were performed in compliance with institutional guidelines and were approved by the Institutional Animal Care and Use Committee of the Cleveland Clinic (protocol 2019-2195).

Organoid cultures

Organoids were formed as previously described (Hubert et al., 2016) by suspending tumor cells in 80% Matrigel (BD Biosciences) and forming 20 µl pearls on parafilm molds prior to culture. Organoids were seeded with 10,000 cells per organoid (30,000 for screen) and cultured in 6-well or 10-cm plates with shaking in Neurobasal™ medium (Gibco) with 1X B-27 supplement (Gibco), 1 mmol/L sodium pyruvate, 2 mmol/L L-glutamine, 50 U/mL penicillin/streptomycin, 20 ng/ml human (h)EGF and 20 ng/ml hFGF2

(R&D systems). Organoids were regionally labeled with CellTracker Blue CMAC (Molecular Probes) for 2 hrs as previously described (Shakya et al., 2021),

Primary cell cultures

Cancer stem cell (CSC) models were generated by passaging primary tumor cells as GBM xenografts as previous described (Lathia et al., 2010). Briefly, primary tumor cells were intracranially implanted into NSG mice, and upon tumor formation, tumors were isolated, digested with papain (Worthington) as described previously (Alvarado et al., 2017), and dissociated cells were plated overnight in Neurobasal™ medium minus phenol red (Gibco) with 1X B-27 supplement (Gibco), 1 mmol/L sodium pyruvate, 2 mmol/L L-glutamine, 50 U/mL penicillin/streptomycin, 20 ng/ml hEGF and 20 ng/ml hFGF2 (R&D systems). Subsequently, CD133+ cells were isolated by magnetic bead sorting (Miltenyi). CD133+ cells were cultured nonadherently in the media described above. Some cell models were previously established at other institutions (**Table 1**). CD133+ cells were seeded in suspension culture at $5x10^4$ cells/ml. CSCs were used for experiments were passaged fewer than 10 times *ex vivo*. After 10 passages, cells were re-implanted into NSG mice and enriched for CD133+ cells. Cells were grown at 37°C with 5% CO_2. De-identified GBM specimens collected from the Cleveland Clinic Brain Tumor and Neuro-Oncology Center were in accordance with an Institutional Review Board-approved protocol, and informed consent was obtained from all GBM patients contributing tumor specimens.

Transformed human neural stem cells were generated as previously described in the CB660 NSC line (Hubert *et al.*, 2013). These include NSC-CB660 cells with dominant-negative p53DD and hTERT (PhT); NSC-CB660 cells with dominant-negative $p53^{DD}$, hTERT, CyclinD1 and $CDK4^{R24C}$ (PhTCC); NSC-CB660 + PhTCC + Myc; NSC-CB660 + PhTCC + H-RasV12; and NSC-CB660 + PhTCC + Myc + H-RasV12. These lines as well as unmodified CB660 cells and U5 cells were grown adherently on plates coated with 10 µg/ml laminin (Sigma) and cultured in a 1:1 ratio of DMEM-F12 and NeuroCult NS-A Basal Medium (Human) (Stem Cell Technologies) with 1X N-2 supplement (Gibco), 1X B-27 supplement, sodium pyruvate, L-glutamine, 1X pen/strep, 20 ng/ml human (h)EGF and 20 ng/ml hFGF2. Isolation and expansion of primary mouse astrocytic stem cells was performed as described in (Marshall et al., 2006).

METHOD DETAILS

Organoid IHC for SOX2/pHH3

Organoids were treated with inhibitors as indicated while shaking in 6-well plates. Treated organoids were then fixed in 10% neutral buffered formalin for at least 24 hrs prior to transfer to 70% ethanol and subsequent paraffin embedding by the LRI Biomedical Engineering histology core. Sections (4 µm) were cut, placed on slides, deparaffinized, unmasked by boiling in 1X citrate solution (Cell Signaling) and blocked with normal donkey serum or BSA. Antigens were detected using anti-SOX2 and anti-phospho-Histone H3 antibodies. Detection was performed with DAB and counterstained with Gills 2 Hematoxylin and bluing reagent. Coverslips were mounted with Permount, and whole slides were scanned on a Leica Aperio AT2 digital slide scanner using a 20X objective in the LRI imaging core. For immunofluorescence, DAPI (1:10,000) was used for DNA detection and images were acquired with the Leica DM5500B upright microscope and Leica DFC 7000 GT monochrome camera (Leica Biosystems). Image fields were extracted using Leica ImageScope software.

CRISPR experiments

CRISPR-Cas9:gRNA delivery and insertion-deletion mutation formation was performed and assessed as described in (Hoellerbauer et al., 2020). CD8A, not expected to be expressed in GBM, was used as a genome cutting control in these experiments. Briefly, ribonucleoprotein (RNP) complexes composed of purified spCas9 and chemically synthesized, 2'-*O*-methyl-3'phosphorothioate-modified sgRNAs (Synthego) were formed and nucleofected into cells using the SG Cell Line 96-well Nucleofector™ Kit and Amaxa 4D Nucleofector X unit (EN-138 program). Cells were pelleted 7 days after nucleofection and

genomic DNA was isolated using the E.Z.N.A. MicroElute Genomic DNA Kit. PCR amplification using Phusion High-Fidelity DNA Polymerase was performed in the region surrounding the predicted cut site(s). Indel formation was assessed using the Synthego ICE tool (ice.synthego.com) after purification of PCR reactions with Monarch PCR & DNA Cleanup Kit (NEB).

Chemical synthesis & WDR5 time-resolved fluorescence energy transfer (TR-FRET) competition assay

Compound 16 (C16) was synthesized as previously published (Tian *et al.*, 2020). Recombinant His6-SUMO-WDR5 was expressed and purified as previously published (Tian et al., 2020). The WDR5 TR-FRET Competition Assay was run following previously published methods (Tian et al., 2020). C16 was tested for 10-mer-Thr-FAM probe displacement using a 10-point concentration response curve with a top concentration of 10 μM and 5-fold dilution scheme. The 520/495 FRET ratio was plotted against compound concentration and fit with a "One Site – Fit Ki" in PRISM 8, with "HotNM" constrained to 150 nM and the "HotKdNM" constrained to 2 nM. C16 was tested in three independent experiments with duplicates run for each experiment (n=6 total).

Western blotting & co-immunoprecipitation

For protein isolation, cells were washed out of medium with PBS. Lysates were prepared using modified radioimmunoprecipitation assay (RIPA) buffer containing protease and phosphatase inhibitors (50 mM Tris-HCl, pH 7.4, 1% NP-40 (vol/vol), 0.25% Na-deoxycholate (wt/vol), 150 mM NaCl, 1 mM EDTA, 1X Sigma p8340 Protease Inhibitor Cocktail, Sigma p5726 Phosphatase Inhibitor Cocktail, 1 mM NaF, 1 mM PMSF). Cells were lysed for 30 min on ice and centrifuged at maximum speed in a tabletop centrifuge to remove debris. Protein concentration was measured on a spectrophotometer (read at 595 nm) using Bradford reagent (Bio-Rad). SDS-PAGE was performed, and cell lysates were resolved on polyacrylamide gels. Proteins were transferred onto PVDF membranes and blocked with TBST+5% BSA. A ChemiDoc MP imaging system (Bio-Rad) was used for visualization. For co-immunoprecipitation experiments, lysates were prepared as described above. Protein lysate (500 μg) was incubated with 5 μg immunoprecipitation antibody at 4°C overnight with rotation followed by incubated with protein A/G agarose beads (Santa Cruz) for 1 hour at 4°C with rotation. Beads were washed 5 times with RIPA buffer, and bead-bound proteins were isolated by boiling antibody-bead complexes in SDS sample buffer. Immunoblotting was performed as described above. For C16 treatment western blots and co-immunoprecipitation, cells were plated at $5x10^5$ cells/ml with the indicated concentrations of inhibitor.

Real-Time Reverse Transcription Polymerase Chain Reaction

RNA was isolated from cells using the Direct-zol RNA miniprep kit (Zymo Research). cDNA was synthesized with Superscript IV First Strand Synthesis System using dT primers (Invitrogen). qPCR was performed using SYBR-Green Mastermix (SA Biosciences) on a Quantstudio Flex 7 Real-Time PCR system using primers listed in the resources table below. Ct values for each gene were normalized to Actin levels and to DMSO treated cells.

Limiting dilution analysis

Cells were plated at 100 cells per well in 12 wells of a 96-well plate, and two-fold serial dilutions were performed. Twelve wells of each cell dose were plated. Limiting-dilution plots and stem-cell frequencies were calculated using ELDA analysis (Hu and Smyth, 2009). For LDAs with C16 treatment, cells were incubated with inhibitor for the duration of the experiment.

IC_{50}, cell growth, viability, apoptosis

Inhibitors were reconstituted to 10 mM in DMSO. For IC_{50} determination, cells were plated at 20,000 cells/ml in Geltrex-coated 96-well plates (to promote adherence) and treated with a 9 point, 2- or 3-fold serial dilution of inhibitor. For IC_{50} calculations, normalization was performed relative to the DMSO condition (100%) and a well with no cells (0%). After 7 days, cell viability was determined by ATP

quantification with the CellTiter-Glo® Luminescent Cell Viability Assay (Promega). For cell growth assays, cells were plated at 20,000 cells/ml in Geltrex-coated 96-well plates and treated with different doses of inhibitor, then imaged using the IncuCyte Live Cell Analysis System using the cell-by-cell module (Sartorius). For apoptosis assays, cells were plated in duplicate plates at 20,000 cells/ml in Geltrex-coated 96-well plates and treated with different doses of inhibitor. Caspase 3/7 activity was determined with the Caspase-Glo 3/7 assay (Promega), and caspase activity was normalized to cell number by performing the CellTiter Glo Luminescent Cell Viability Assay on the duplicate plate. For quantification of apoptosis over time, cells were plated at 20,000 cells/ml in Geltrex-coated 96-well plates and treated with different doses of inhibitor in the presence of 1:1000 IncuCyte® Caspase-3/7 Dye for Apoptosis (Sartorius). Doubling times were calculated by determining cell counts over multiple days with the IncuCyte Live Cell Analysis System cell-by-cell module (Sartorius).

BBB penetration potential using MDR1-MDCK cell monolayers

MDR1-MDCK cell monolayers were grown to confluence on collagen-coated microporous membranes in 12-well assay plates. The permeability assay buffer was Hanks' balanced salt solution containing 10 mM HEPES and 15 mM glucose at a pH of 7.4. The buffer in the receiver chamber also contained 1% bovine serum albumin. The dosing solution concentration was 5 µM of C16 in the assay buffer. Cell monolayers were dosed on the apical side (A-to-B) or basolateral side (B-to-A) and incubated at 37°C with 5% CO_2 in a humidified incubator. Samples were taken from the donor and receiver chambers at 120 minutes. Each determination was performed in duplicate. All samples were assayed by LC-MS/MS using electrospray ionization. Further details can be found at Absorption.com, assay #EA203.

***In vivo* brain:plasma study and toxicity studies in mice**

C16 was formulated from powder as 2 mg/mL solution in a 20% 2-(hydroxypropyl)-β-cyclodextrin in ddH_2O (HP-β-CD; Sigma) solution. The solution was then made acidic with 1.0 equivalent of aqueous 1N HCl. The mixture was vortexed briefly and then sonicated for 5 min in a room temperature water bath sonicator to afford a clear solution to fine microsuspension. Animals were injected intraperitoneally (IP) with a maximal dosing volume of 5 mL/kg to give a final 10 mg/kg body weight dose.

Male CD-1 mice (Charles River Laboratories, Wilmington, MA) were overnight fasted on the evening prior to study (food removed between 1500-1600 h). On the morning of study, mice were weighed and allowed to acclimate to the room for at least 30 min prior to dosing. Food was returned 3 hrs after injection. At time 0, an IP injection of C16 was given. At 0.5 h, 1 h, 3 hrs, and 6 hrs after injection (n=2 per time point), mice were placed into a plane of anesthesia using isoflurane. A terminal blood sample was collected via cardiac puncture followed by immediate euthanasia and brain collection. Brain was washed with cold PBS or Saline, blotted dry on a piece of gauze, weighed, and flash frozen in liquid Nitrogen. Whole blood was centrifuged at 5000-6000 g for 5 minutes and plasma was removed into a fresh tube for storage. All samples were stored at -80°C until shipment on dry ice to Q2 Solutions for tissue distribution bioanalysis (Q2 Solutions Bioanalytical and ADME Laboratories, Indianapolis, IN). The plotted time-course exposure plot for C16 represents the average concentrations of processed brain and plasma samples (brain homogenate supernatant and plasma) as determined by LC-MS/MS.

Intracranial implantation

Intracranial tumor implantations were performed as described previously (Bayik et al., 2020). NSG mice were anesthetized with inhaled isoflurane for the duration of the procedure. For shRNA experiments, a total of 10,000 DI318 CSCs infected with control or WDR5 shRNAs were suspended in 10 µl Neurobasal null medium and stereotactically implanted in the left hemisphere ~2.5 mm deep into the brain. For drug treatment experiments, a total of 5,000 DI318 CSCs were implanted intracranially into mice, and 10 days later, 10 mg/kg C16 was injected IP daily (formulated as described in "*In vivo* brain:plasma study in mice" section). Mice were monitored for neurologic signs and weight loss and deemed at endpoint when exhibiting any of these symptoms.

Flank tumor experiments
NSG mice were implanted subcutaneously with 500,000 DI318 or L0 human GBM CSCs. After tumor formation (3 weeks for DI318, 10 weeks for L0), 3 mg/kg C16 was injected daily directly into the tumors or 10 mg/kg C16 was injected daily intraperitoneally as indicated. For intratumoral dosing, C16 was dissolved at 5.1 mg/ml in 17.5% DMSO in PBS and treatment was started 3 weeks after tumor cell injection when tumors reached a volume of ~100mm^3. Tumor volume was calculated using the following formula for ellipsoid volume: $4/3\pi(w/2)^2(h/2)$. For intraperitoneal (IP) dosing, C16 was dissolved at 2 mg/ml in 20% HP-β-CD in ddH2O as described in "*In vivo* brain:plasma study in mice" section. Treatment was started 10 weeks after tumor cell injection when tumors reached a volume of ~500mm^3. When any animals in the experiment reached endpoint (determined by tumor size), mice were euthanized.

WDR5 knockdown
MISSION® pLKO.1-puro Non-Mammalian shRNA (SHC002) and WDR5 knockdown plasmids were purchased from Sigma. Several clones were tested, and 2 non-overlapping clones with efficient knockdown were selected to produce lentiviral particles (TRC clone IDs: TRCN0000157812 (shWDR5#12) and TRCN0000118047 (shWDR5#47)). For virus production, pLKO.1-shRNA plasmids were transfected into 293T cells along with psPAX2 and pMD2.G packaging plasmids to produce lentivirus. Forty-eight and 72 hrs after transfection, supernatant containing lentiviral particles was collected and concentrated with PEGit virus precipitation solution according to manufacturer's protocol (System Biosciences). CSCs were plated on Geltrex, and virus was added to culture medium (MOI = 2), then cells with virus integration were selected with 2-4 μg/ml puromycin.

QUANTIFICATION AND STATISTICAL ANALYSIS

Western blot quantification was performed using ImageJ (v1.53k, NIH). For two group comparisons, P values were calculated using unpaired or paired two-tailed t tests. For multiple group comparisons, one-way ANOVA with post hoc tests were used as indicated in the figure legends. Log-rank tests were used for survival analysis. GraphPad Prism 9 was used for statistical tests. All *in vitro* experiments were done in technical triplicates for each experimental group, and multiple independent experiments were performed. To determine the number of mice needed per group for animal experiments, we utilized the Guidelines for the Care and Use of Mammals in Neuroscience and Behavioral Research from the National Research Council to estimate the minimal number necessary to achieve statistical significance ($p < 0.05$) for all tumor growth studies. The number of animals per arm was based upon the following calculation: $= (1 + 2C)\left(\frac{s}{d}\right)^2$, where n = Number of Animals per Experimental Group; C = 9.18 when $\alpha = 0.05$ and $1 - \beta = 0.85$ (Significance level of 5% with a power of 85%); s = Standard Deviation (≈ 7 days); d = Difference to be Detected (≥ 10 days). Thus, n = 10 animals were used per group, and to control for sexual dimorphism, males and females were treated as separate experimental groups and combined if there were no differences in the measured outcomes. n represents independent experiments (biological replicates) or individual mice. Statistical details can be found in figure legends. $p<0.05$ was considered statistically significant. *, $p < 0.05$; **, $p < 0.01$; ***, $p < 0.001$; ****, $p < 0.0001$.

CUT&Tag bioinformatic analysis
CUT&Tag reads were aligned to the human genome (hg38) using Bowtie2 (Langmead and Salzberg, 2012) as previously described (Henikoff et al., 2020). MACS2 was used for peak calling (Zhang *et al.*, 2008) and peaks were annotated using ChIPseeker (Yu *et al.*, 2015). BedTools (Quinlan and Hall, 2010), DiffBind (Ross-Innes *et al.*, 2012) and DESeq2 (Love *et al.*, 2014) were utilized to identify unique peaks, consensus peaks and perform differential analysis between groups (with significance set to False Discovery Rate (FDR) < 0.05). Fastq files and narrow peak files for each sample were deposited in GEO (GSE199110).

Brain tumor & normal brain gene expression data and analysis

Bulk RNA sequencing data from normal brain cell types and GBM CSC lines was obtained from (Toledo *et al.*, 2015). For the BRAIN-UMAP, brain tumor and normal gene expression data were obtained from Children's Brain Tumor Network (Ijaz et al., 2020), CGGA (Zhao et al., 2021), GTEX (Consortium, 2020), and TCGA (Cancer Genome Atlas Research Network, 2008). Log2 TPM normalized batch corrected gene expression values for protein coding genes were subjected to uniform manifold approximation and projection (UMAP) dimension reduction to create a reference landscape. A detailed description of creation of the analysis pipeline is available in (Arora et al., 2023). The reference landscape was colored in by gene expression value for genes of interest. T-tests were performed in base R using the batch corrected log2 TPM gene expression values to test if the mean in one group was greater than the mean in the other group. The BRAIN-UMAP reference landscape can be accessed via the open-source tool Oncoscape. (https://oncoscape.sttrcancer.org/#project_bulkrnaseqbrainumap).

RESOURCE AVAILABILITY

Further information and requests for resources and reagents should be directed to and will be fulfilled by the corresponding authors, Justin D. Lathia (lathiaj@ccf.org) and Christopher G. Hubert (christopher.hubert@case.edu).

Supplemental References

Alvarado, A.G., Thiagarajan, P.S., Mulkearns-Hubert, E.E., Silver, D.J., Hale, J.S., Alban, T.J., Turaga, S.M., Jarrar, A., Reizes, O., Longworth, M.S., et al. (2017). Glioblastoma Cancer Stem Cells Evade Innate Immune Suppression of Self-Renewal through Reduced TLR4 Expression. Cell Stem Cell *20*, 450-461 e454. 10.1016/j.stem.2016.12.001.

Arora, S., Szulzewsky, F., Jensen, M., Nuechterlein, N., Pattwell, S.S., and Holland, E.C. (2023). An RNA seq-based reference landscape of human normal and neoplastic brain. bioRxiv, 2023.2001.2003.522658. 10.1101/2023.01.03.522658.

Bayik, D., Zhou, Y., Park, C., Hong, C., Vail, D., Silver, D.J., Lauko, A., Roversi, G., Watson, D.C., Lo, A., et al. (2020). Myeloid-Derived Suppressor Cell Subsets Drive Glioblastoma Growth in a Sex-Specific Manner. Cancer Discov *10*, 1210-1225. 10.1158/2159-8290.CD-19-1355.

Bowman, R.L., Wang, Q., Carro, A., Verhaak, R.G.W., and Squatrito, M. (2017). GlioVis data portal for visualization and analysis of brain tumor expression datasets. Neuro-Oncology *19*, 139-141. 10.1093/neuonc/now247.

Cancer Genome Atlas Research Network (2008). Comprehensive genomic characterization defines human glioblastoma genes and core pathways. Nature *455*, 1061-1068. nature07385 [pii]

10.1038/nature07385.

Consortium, G.T. (2020). The GTEx Consortium atlas of genetic regulatory effects across human tissues. Science *369*, 1318-1330. 10.1126/science.aaz1776.

Dempster, J.M., Rossen, J., Kazachkova, M., Pan, J., Kugener, G., Root, D.E., and Tsherniak, A. (2019). Extracting Biological Insights from the Project Achilles Genome-Scale CRISPR Screens in Cancer Cell Lines. bioRxiv, 720243. 10.1101/720243.

Ghandi, M., Huang, F.W., Jane-Valbuena, J., Kryukov, G.V., Lo, C.C., McDonald, E.R., 3rd, Barretina, J., Gelfand, E.T., Bielski, C.M., Li, H., et al. (2019). Next-generation characterization of the Cancer Cell Line Encyclopedia. Nature *569*, 503-508. 10.1038/s41586-019-1186-3.

Haller, F., Happel, N., Schulten, H.J., von Heydebreck, A., Schwager, S., Armbrust, T., Langer, C., Gunawan, B., Doenecke, D., and Fuzesi, L. (2007). Site-dependent differential KIT and PDGFRA expression in gastric and intestinal gastrointestinal stromal tumors. Mod Pathol *20*, 1103-1111. 10.1038/modpathol.3800947.

He, W., Huang, L., Li, M., Yang, Y., Chen, Z., and Shen, X. (2017). MiR-148b, MiR-152/ALCAM Axis Regulates the Proliferation and Invasion of Pituitary Adenomas Cells. Cell Physiol Biochem *44*, 792-803. 10.1159/000485342.

Heinz, S., Benner, C., Spann, N., Bertolino, E., Lin, Y.C., Laslo, P., Cheng, J.X., Murre, C., Singh, H., and Glass, C.K. (2010). Simple combinations of lineage-determining transcription factors prime cis-regulatory elements required for macrophage and B cell identities. Mol Cell *38*, 576-589. 10.1016/j.molcel.2010.05.004.

Henikoff, S., Henikoff, J.G., Kaya-Okur, H.S., and Ahmad, K. (2020). Efficient chromatin accessibility mapping in situ by nucleosome-tethered tagmentation. Elife *9*. 10.7554/eLife.63274.

Hoellerbauer, P., Kufeld, M., and Paddison, P.J. (2020). Efficient Multi-Allelic Genome Editing of Primary Cell Cultures via CRISPR-Cas9 Ribonucleoprotein Nucleofection. Curr Protoc Stem Cell Biol *54*, e126. 10.1002/cpsc.126.

Hu, Y., and Smyth, G.K. (2009). ELDA: extreme limiting dilution analysis for comparing depleted and enriched populations in stem cell and other assays. J Immunol Methods *347*, 70-78. 10.1016/j.jim.2009.06.008.

Hubert, C.G., Bradley, R.K., Ding, Y., Toledo, C.M., Herman, J., Skutt-Kakaria, K., Girard, E.J., Davison, J., Berndt, J., Corrin, P., et al. (2013). Genome-wide RNAi screens in human brain tumor isolates reveal a novel viability requirement for PHF5A. Genes Dev *27*, 1032-1045. 10.1101/gad.212548.112.

Hubert, C.G., Rivera, M., Spangler, L.C., Wu, Q., Mack, S.C., Prager, B.C., Couce, M., McLendon, R.E., Sloan, A.E., and Rich, J.N. (2016). A Three-Dimensional Organoid Culture System Derived from Human Glioblastomas Recapitulates the Hypoxic Gradients and Cancer Stem Cell Heterogeneity of Tumors Found In Vivo. Cancer Res *76*, 2465-2477. 10.1158/0008-5472.CAN-15-2402.

Ijaz, H., Koptyra, M., Gaonkar, K.S., Rokita, J.L., Baubet, V.P., Tauhid, L., Zhu, Y., Brown, M., Lopez, G., Zhang, B., et al. (2020). Pediatric high-grade glioma resources from the Children's Brain Tumor Tissue Consortium. Neuro Oncol *22*, 163-165. 10.1093/neuonc/noz192.

Jiang, D., He, Y., Mo, Q., Liu, E., Li, X., Huang, L., Zhang, Q., Chen, F., Li, Y., and Shao, H. (2021). PRICKLE1, a Wnt/PCP signaling component, is overexpressed and associated with inferior prognosis in acute myeloid leukemia. J Transl Med *19*, 211. 10.1186/s12967-021-02873-8.

Kuppers, D.A., Linton, J., Espinosa, S.O., McKenna, K.M., Rongvaux, A., and Paddison, P.J. (2022). Gene knock-outs in human CD34+ hematopoietic stem and progenitor cells and in the human immune system of mice. bioRxiv, 2022.2010.2006.511235. 10.1101/2022.10.06.511235.

Langmead, B., and Salzberg, S.L. (2012). Fast gapped-read alignment with Bowtie 2. Nat Methods *9*, 357-359. 10.1038/nmeth.1923.

Lathia, J.D., Gallagher, J., Heddleston, J.M., Wang, J., Eyler, C.E., Macswords, J., Wu, Q., Vasanji, A., McLendon, R.E., Hjelmeland, A.B., and Rich, J.N. (2010). Integrin alpha 6 regulates glioblastoma stem cells. Cell Stem Cell *6*, 421-432. 10.1016/j.stem.2010.02.018.

Li, H., Handsaker, B., Wysoker, A., Fennell, T., Ruan, J., Homer, N., Marth, G., Abecasis, G., Durbin, R., and Genome Project Data Processing, S. (2009). The Sequence Alignment/Map format and SAMtools. Bioinformatics *25*, 2078-2079. 10.1093/bioinformatics/btp352.

Ling, X.H., Fu, H., Chen, Z.Y., Lu, J.M., Zhuo, Y.J., Chen, J.H., Zhong, W.D., and Jia, Z. (2019). miR-505 suppresses prostate cancer progression by targeting NRCAM. Oncol Rep *42*, 991-1004. 10.3892/or.2019.7231.

Love, M.I., Huber, W., and Anders, S. (2014). Moderated estimation of fold change and dispersion for RNA-seq data with DESeq2. Genome Biol *15*, 550. 10.1186/s13059-014-0550-8.

Luo, B., Cheung, H.W., Subramanian, A., Sharifnia, T., Okamoto, M., Yang, X., Hinkle, G., Boehm, J.S., Beroukhim, R., Weir, B.A., et al. (2008). Highly parallel identification of essential genes in cancer cells. Proc Natl Acad Sci U S A *105*, 20380-20385. 10.1073/pnas.0810485105.

Marshall, G.P., 2nd, Laywell, E.D., Zheng, T., Steindler, D.A., and Scott, E.W. (2006). In vitro-derived "neural stem cells" function as neural progenitors without the capacity for self-renewal. Stem cells (Dayton, Ohio) *24*, 731-738. 10.1634/stemcells.2005-0245.

Meyers, R.M., Bryan, J.G., McFarland, J.M., Weir, B.A., Sizemore, A.E., Xu, H., Dharia, N.V., Montgomery, P.G., Cowley, G.S., Pantel, S., et al. (2017). Computational correction of copy number effect improves specificity of CRISPR-Cas9 essentiality screens in cancer cells. Nat Genet *49*, 1779-1784. 10.1038/ng.3984.

Miller, T.E., Liau, B.B., Wallace, L.C., Morton, A.R., Xie, Q., Dixit, D., Factor, D.C., Kim, L.J.Y., Morrow, J.J., Wu, Q., et al. (2017). Transcription elongation factors represent in vivo cancer dependencies in glioblastoma. Nature *547*, 355-359. 10.1038/nature23000.

Pan, Z., Wu, C., Li, Y., Li, H., An, Y., Wang, G., Dai, J., and Wang, Q. (2020). LncRNA DANCR silence inhibits SOX5-medicated progression and autophagy in osteosarcoma via regulating miR-216a-5p. Biomed Pharmacother *122*, 109707. 10.1016/j.biopha.2019.109707.

Quinlan, A.R., and Hall, I.M. (2010). BEDTools: a flexible suite of utilities for comparing genomic features. Bioinformatics *26*, 841-842. 10.1093/bioinformatics/btq033.

Ross-Innes, C.S., Stark, R., Teschendorff, A.E., Holmes, K.A., Ali, H.R., Dunning, M.J., Brown, G.D., Gojis, O., Ellis, I.O., Green, A.R., et al. (2012). Differential oestrogen receptor binding is associated with clinical outcome in breast cancer. Nature *481*, 389-393. 10.1038/nature10730.

Shakya, S., Gromovsky, A.D., Hale, J.S., Knudsen, A.M., Prager, B., Wallace, L.C., Penalva, L.O.F., Brown, H.A., Kristensen, B.W., Rich, J.N., et al. (2021). Altered lipid metabolism marks glioblastoma stem and non-stem cells in separate tumor niches. Acta Neuropathol Commun *9*, 101. 10.1186/s40478-021-01205-7.

Shin, J., Tkachenko, S., Chaklader, M., Pletz, C., Singh, K., Bulut, G.B., Han, Y.M., Mitchell, K., Baylis, R.A., Kuzmin, A.A., et al. (2022). Endothelial OCT4 is atheroprotective by preventing metabolic and phenotypic dysfunction. Cardiovasc Res *118*, 2458-2477. 10.1093/cvr/cvac036.

Tang, B., Raviv, A., Esposito, D., Flanders, K.C., Daniel, C., Nghiem, B.T., Garfield, S., Lim, L., Mannan, P., Robles, A.I., et al. (2015). A flexible reporter system for direct observation and isolation of cancer stem cells. Stem Cell Reports *4*, 155-169. 10.1016/j.stemcr.2014.11.002.

Tian, J., Teuscher, K.B., Aho, E.R., Alvarado, J.R., Mills, J.J., Meyers, K.M., Gogliotti, R.D., Han, C., Macdonald, J.D., Sai, J., et al. (2020). Discovery and Structure-Based Optimization of Potent and Selective WD Repeat Domain 5 (WDR5) Inhibitors Containing a Dihydroisoquinolinone Bicyclic Core. J Med Chem *63*, 656-675. 10.1021/acs.jmedchem.9b01608.

Toledo, C.M., Ding, Y., Hoellerbauer, P., Davis, R.J., Basom, R., Girard, E.J., Lee, E., Corrin, P., Hart, T., Bolouri, H., et al. (2015). Genome-wide CRISPR-Cas9 Screens Reveal Loss of Redundancy between PKMYT1 and WEE1 in Glioblastoma Stem-like Cells. Cell Rep *13*, 2425-2439. 10.1016/j.celrep.2015.11.021.

Yu, G., Wang, L.G., and He, Q.Y. (2015). ChIPseeker: an R/Bioconductor package for ChIP peak annotation, comparison and visualization. Bioinformatics *31*, 2382-2383. 10.1093/bioinformatics/btv145.

Zhang, Y., Liu, T., Meyer, C.A., Eeckhoute, J., Johnson, D.S., Bernstein, B.E., Nusbaum, C., Myers, R.M., Brown, M., Li, W., and Liu, X.S. (2008). Model-based analysis of ChIP-Seq (MACS). Genome Biol *9*, R137. 10.1186/gb-2008-9-9-r137.

Zhao, Z., Zhang, K.N., Wang, Q., Li, G., Zeng, F., Zhang, Y., Wu, F., Chai, R., Wang, Z., Zhang, C., et al. (2021). Chinese Glioma Genome Atlas (CGGA): A Comprehensive Resource with Functional Genomic Data from Chinese Glioma Patients. Genomics Proteomics Bioinformatics *19*, 1-12. 10.1016/j.gpb.2020.10.005.